An optical study of Ni induced crystallization of a-Si thin films

2007 J. Phys.: Condens. Matter 19 496208

(http://iopscience.iop.org/0953-8984/19/49/496208)

IOP PUBLISHING JOURNAL OF PHYSICS: CONDENSED MATTER

J. Phys.: Condens. Matter **19** (2007) 496208 (11pp) doi:10.1088/0953-8984/19/49/496208

An optical study of Ni induced crystallization of a-Si thin films

Koppolu Uma Mahendra Kumar[1], Rajeeb Brahma[1], M Ghanashyam Krishna[1], Anil K Bhatnagar[1] and G Dalba[2]

[1] School of Physics, University of Hyderabad, Gachibowli, Hyderabad 46, India
[2] Department of Physics, University of Trento, 38050 POVO (Trento), Italy

E-mail: mgksp@uohyd.ernet.in

Received 17 August 2007, in final form 16 October 2007
Published 12 November 2007
Online at stacks.iop.org/JPhysCM/19/496208

Abstract

The optical properties of nanocrystalline silicon (nc-Si), formed by nickel (Ni) induced crystallization of amorphous silicon (a-Si) films, are presented. Growth of nc-Si was characterized by Raman spectroscopy and UV–vis–NIR spectrophotometry. Significantly, the onset of crystallization occurred at 600 °C within 15 min of annealing, as evidenced from the Raman peak centered at 514 cm^{-1}. It is demonstrated that the shape of the optical absorption spectrum is a function of thickness, substrate temperature, topological disorder and metal content in the films. Ni doping of the films results in optical inhomogeneity in the films and therefore anomalous dispersion in the behavior of the refractive index. It is further shown that these parameters also influence the position of the Urbach edges. The present study shows that metal induced crystallization of a-Si does not require extended durations of annealing and that the crystallization process is accompanied by structural, chemical and microstructural inhomogeneity in the films.

(Some figures in this article are in colour only in the electronic version)

1. Introduction

The quest for device quality polycrystalline silicon (poly-Si) for developing display elements driven by thin-film transistors based on the active matrix system on glass and flexible substrates is a topic of great current interest [1]. This is mainly because such devices would become more cost effective and therefore more attractive for applications. The crystallization of Si at temperatures that are sufficiently low (<600 °C) to be compatible with the processing of softer materials is central to these developments. Solid phase crystallization (SPC) is one of a number of different crystallization methods adopted for amorphous silicon (a-Si), and was first reported by Mayer *et al* [2]. This process demands typical temperatures of 600–700 °C. Apart from SPC, rapid thermal annealing (RTA) [3] and laser annealing (LA) [4] are other techniques adopted for

the crystallization of a-Si. Metal induced crystallization (MIC) emerged as a viable technique for crystallization of a-Si films as a result of various attempts to decrease the crystallization temperature, shorten the crystallization time and increase grain size uniformity. This was first introduced by Liu and Fonash in 1993 [5] as an approach to fabricate polycrystalline silicon thin-film transistors by inserting a thin, discontinuous Pd layer between the substrate and the a-Si precursor. During annealing, the Pd reacted to form a silicide seed layer, reducing the crystallization time, at 600 °C, from tens of hours to 2 h. Since then, metals like Al, Mo, Ni and Ti [6] have been used to achieve MIC. Of these, Ni and Al have been more extensively studied than the other metals. In the case of aluminum induced crystallization (AIC) a large tensile strain is induced in the silicon lattice, whereas Ni offers less strain and better electrical properties ([7] and references therein). In the case of Ni, nucleation and growth of crystalline silicon are mediated by formation of $NiSi_2$ and the transformation rate is limited by diffusion of $NiSi_2$. Since the lattice constant of the $NiSi_2$ phase is very close to that of Si, this phase can lead to the crystallization of amorphous silicon at a relatively low temperature. These crystalline seeds (metal silicide phase) can also propagate into the metal-free area by thermal diffusion through a process called metal induced lateral crystallization (MILC) [8], thus producing good quality poly-Si films without metal contamination. Crystallization by MILC, however, takes a relatively longer time than MIC since the slow diffusion process determines the crystallization velocity.

A survey of the literature shows that a detailed study of the optical properties of Ni doped crystalline Si by the MIC process is still lacking. The refractive indices of the Ni doped Si films are not known and it is also not very well understood whether the optical band gap is affected by the MIC process. Furthermore, it is not clear whether the diffusion of Ni into Si causes optical inhomogeneities. The variation in band structure due to the MIC process has also not been studied in detail. It is important to understand these properties of MIC-Si since most of the applications envisaged are photonic or optoelectronic in nature. The motivation of the current work is, therefore, to understand the evolution of optical properties such as spectral transmission, specular reflectance, refractive index, band gap and Raman scattering phenomena as a function of processing parameters and thickness of a-Si films doped with Ni during crystallization. The optical probes employed are Raman spectroscopy and UV–vis–NIR spectrophotometry. A detailed optical study of the crystallization process of a-Si thin films has been carried out and a model for the diffusion of Ni into Si and the consequent crystallization of amorphous Si is proposed.

2. Experiment

The nickel and silicon films were deposited by resistive thermal evaporation from a tungsten spiral and tantalum boat, respectively. The vacuum chamber was evacuated using a diffusion–rotary pump combination equipped with a liquid nitrogen trap. The base pressure was 1×10^{-6} Torr. In all cases the substrate to source distance was kept constant at 5 cm. The starting materials were granular pure silicon powder (99.999%) and nickel wire (99.99% pure). The samples used in this study were thin films of a-Si deposited in two sets on fused silica. One set of samples was prepared on substrates which were held at ambient temperature, and the second set was prepared maintaining the substrate temperature (T_s) at 350 °C during deposition. After recording the spectral transmission curves, these films were coated with a 50 nm thin nickel blanket top layer to form a Ni/Si/silica stack. The thickness of the Si films was varied from 100 to 1100 nm and the deposition rate was maintained constant at 1 nm s^{-1}. The thickness was measured *in situ* by a quartz crystal monitor and, after deposition, using a surface profilometer (model XP-1 Ambios Tech., USA) as well as calculation from the

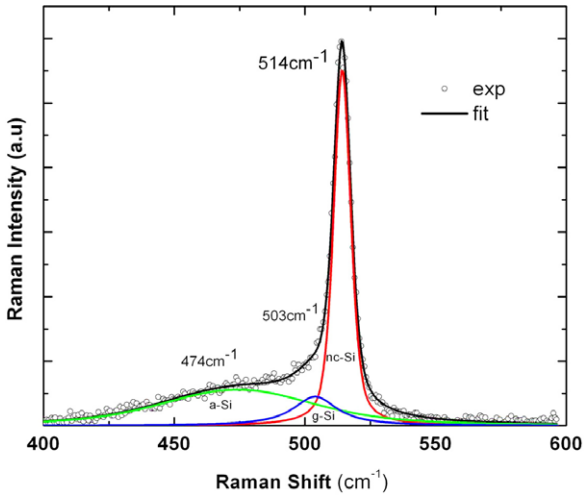

Figure 1. Raman spectra from a-Si thin film containing nc-Si after annealing at $T = 600\,^{\circ}\mathrm{C}$ with 4.5% of Ni. Individual components of line shape are assigned to scattering contributions from amorphous (474 cm^{-1}), nanocrystalline (514 cm^{-1}) and grain boundaries (503 cm^{-1}).

spectral transmission curves [9]. The films were annealed in a furnace atmosphere (in air) at 600 °C. Before and after annealing, the films were characterized for transmission and specular reflectance in the wavelength range 190–2500 nm by means of a dual-beam spectrophotometer (UV–vis–NIR, model, Jasco V-570) having a resolution limit of ±0.2 nm and a sampling interval of 2 nm. All the samples were measured at the same incidence angle of $6.0^{\circ} \pm 0.1$ in order to avoid any fringe shift due to angular discrepancy. The transmitted intensities were measured to an accuracy of better than 0.3%. The refractive index and extinction coefficients were extracted from the measured spectral curves using techniques described in [10]. The Raman spectra were recorded in air using an argon ion laser in the back scattering geometry in a JY-ISA T64 000 spectrometer equipped with an Olympus BX40 confocal microscope and 100× objective (1 μm diameter focal spot size) with a liquid nitrogen cooled charge coupled device (CCD) detector. The spectral components coming from the amorphous and crystalline components were deconvoluted and related to Raman shifts and peak broadening. After correcting for the base line, a Voigt-like function was used for curve fitting the Raman spectra. Care was taken to optimize the parameters of the He–Ne laser so that it does not induce onset of crystallization in the sample. The phase content with in the samples was investigated in a spectral region 400–600 cm^{-1} with an irradiation time of 300 s.

3. Results and discussion

3.1. Raman spectroscopy

Raman spectra recorded using a micro-Raman spectrometer with a laser wavelength of 514 nm, in the back scattering geometry, are shown in figure 1. The peak at 474 cm^{-1} was assigned to be due to transverse optical (TO) phonons of amorphous silicon [11]. After a conventional furnace annealing at 600 °C for 15 min, a Raman peak with central frequency at 514 cm^{-1} was observed for the Ni doped Si films with a relative Ni concentration of 5%. It is well known that a-Si and crystalline silicon (c-Si) have their Raman frequencies centered at 475 and 520 cm^{-1}. The Raman central frequency at 520 cm^{-1} is the silicon first direct transition, Γ'_{25}–Γ_{15} at 3.3 eV, a feature that has also been observed in specular reflectance curves shown later. A significantly downshifted and asymmetrically broadened peak centered at 514 cm^{-1} was found for nanocrystalline silicon having a crystallite size of 6 ± 2 nm. Nanocrystallinity and quantum

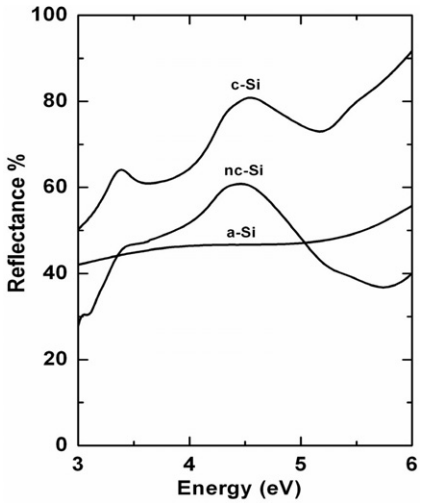

Figure 2. Specular reflectance curves of a-Si film, nc-Si film and c-Si wafer.

confinement have been reported in silicon of many forms, such as Si nanowires, quantum dots and in systems where the lateral dimensions are down to 15 nm [12, 13]. Ritcher *et al* proposed a model for quantum confinement, and Campbell *et al* [14, 15] developed it further. This model has come to be known as the RCF model or phonon confinement model. Pisanec *et al* [16] further improved the model by accounting for the Raman peak position and width in the size and morphology of the nanocrystalline material. According to Schubert *et al* [17], the measured line shape of the Raman signal comprises four different contributions, namely from amorphous, polycrystalline, grain boundaries and nanocrystalline components present in the sample. The whole signal is deconvoluted into individual contributions as shown in figure 1. It is evident from figure 1 that in the Ni induced crystalline sample the contributions from three components can easily be identified. It should be noted that films annealed at temperatures $<600\,^{\circ}$C and higher concentrations of Ni did not show any evidence for crystallinity in the Raman spectra.

3.2. Specular reflectance

Reflectance spectra of crystalline materials show considerable structure in the form of peaks and shoulders as a consequence of optical transitions, and these features are smeared out due to the lack of long-range order in amorphous materials [18]. This difference is indeed observed in the present study, in the case of a-Si and Ni crystallized silicon thin films.

The specular reflectance at near normal incidence (approx. 6°) measured in the energy range of 0.5–6 eV is shown in figure 2. The specular reflectance data of the present work agree well with those of Phillip *et al* [19] within the range of measurement. Amorphous silicon shows a broad halo without any peaks. However, the Ni doped sample showed two peaks, one at 3.2 eV and another at 4.3 eV. The reflectance of a silicon single crystal measured on the same spectrometer shows the same features at 3.34 and 4.5 eV as reported first by Phillip *et al* [18]. In c-Si, this structure is the resultant of band transitions at Γ'_{25}–Γ_{15} and X_4–X_1 [20].

Similar features found in Ni doped silicon in the current study provide clear evidence for crystallization. The large halo in the reflectance of the a-Si films is essentially due to the lack of long-range order. The higher energy parts of c-Si and nc-Si are not similar beyond 5 eV. The thin films in the present study are not chemically homogeneous because of Ni doping and due

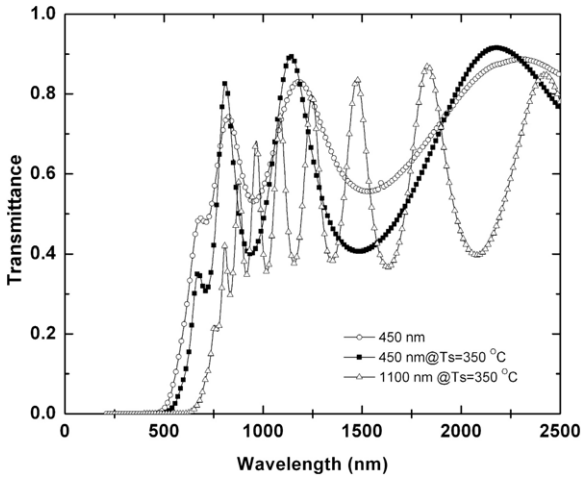

Figure 3. Spectral transmittance of the films of thickness 450 nm, deposited at ambient temperature (open circles), a substrate temperature of 350 °C (closed squares) along with the spectral transmittance curve for the 1100 nm thick film deposited at a substrate temperature of 350 °C (triangles).

to the formation of nickel silicides. This difference is manifested in the reflectance spectra of the a-Si films, in that they exhibit an increase in reflectance beyond 5 eV similar to c-Si but with reduced intensity. This signifies that the reflectance is sensitive to the chemical composition of the sample as well as to its structure. The shift to lower energies of the reflection peaks of nc-Si can also be attributed to the presence of chemical inhomogeneity and a-Si component in the samples. The lower intensities of the peaks may be due to the passive layers formed on the sample surface, as reflectance is sensitive to the surface of the sample.

3.3. Spectral transmittance, Urbach edges and Tauc parameters

The fact that optical transitions are governed by the local atomic order is very well established both in amorphous and crystalline materials. A study of the Urbach energy (E_U) and the Tauc parameter, $B^{1/2}$, enables us to establish a correlation between structural disorder (electronic and topological) and optical properties. While the former can be related to the electronic disorder, the latter is related to the symmetry of the bonding orbital at the top of the valence band maxima (VBM) [21, 22]. These kinds of investigations were followed in the case of a-Si:H films to optimize their electrical properties in conjunction with tailoring their optical properties [23]. In glassy materials there is an absence of long-range order and the existence of short-range order. This would mean that each atom has a definite coordination (number of nearest neighbors) and it will display some deviation in bond lengths and bond angles so that there is no single pattern such as a unit cell which can be repeated to give a three-dimensional solid structure as in crystalline materials. This results in the appearance of localized states in the pseudo-gap that eventually lead to a rise in the absorption edge by several eV as well as to its broadening, as first described by Urbach [24]. The spectral transmission curves for the undoped a-Si films deposited in the current study are shown in figure 3. At a thickness of 450 nm the transmittance of the films in the interference region (about 1000–2500 nm) or in the transparent region is about 90%.

The optical absorption edge as a function of thickness and substrate temperature shifted towards longer wavelengths with a small variation in the refractive index. The shift can be

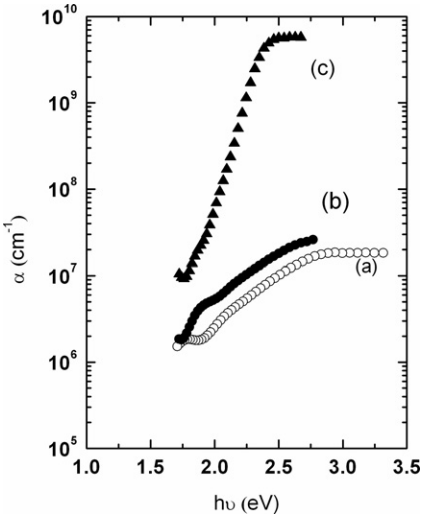

Figure 4. Absorption coefficient of films of thickness 450 nm deposited at (a) ambient temperature, (b) 350 °C and (c) of the 1100 nm thick, annealed Ni doped film.

due to small amorphous Si clusters, oxygen bonds on the surface formed during annealing and may also arise from the micro voids formed during growth. However, for a constant thickness (450 nm) of a-Si film, the shape of the absorption edge, apart from a small increase in the absorption coefficient, is similar both for the films deposited on substrates maintained at ambient temperature and at 350 °C during deposition, as shown in figure 4. Also shown in the same figure is the absorption coefficient for a sample doped with 10% of nickel and annealed to 600 °C after deposition. The a-Si film (figure 4(a)) deposited at ambient temperature showed a broad edge, with an absorption coefficient of about 10^6–10^7 cm^{-1}. The undoped a-Si deposited at a substrate temperature of 350 °C (figure 4(b)) also displayed a similar broadening in the absorption edge but with a larger absorption coefficient due to the changes in the transition matrix element.

The sample doped with nickel (figure 4(c)) had a relatively sharp edge, with a three orders of magnitude increase in its absorption coefficient. The increase in the absorption coefficient can be attributed to the Ni metal component present in the sample and the slope of the edges, signaling the role of Ni in catalyzing the crystallization in silicon, can be quantified by Urbach energies. The appropriate parts of the absorption coefficient were fitted to the following equations.

$$(\alpha\hbar\upsilon)^{\frac{1}{2}} = B^{\frac{1}{2}}(\hbar\upsilon - E_{\text{Tauc}}) \tag{1}$$

$$\alpha = \alpha_0 \exp\left(\frac{E_0 - \hbar\upsilon}{E_{\text{U}}}\right). \tag{2}$$

Here, E_{U} is the Urbach energy, and $B^{1/2}$ is the Tauc parameter. Assuming parabolic valence band and conduction band, the Tauc gap or optical band gap (E_{g}) is determined by plotting $(\alpha h\upsilon)^{1/2}$ against $(h\upsilon)$ and extrapolating the linear region of the curve. The dependence of the Urbach energy, E_{U}, on different concentrations of Ni is plotted in figure 5. The Urbach slope increases with introduction of Ni metal into the a-Si film, both in the doping and alloy regime and up to 4.5% of Ni doping the Urbach energy E_{U} increases without affecting E_{Tauc}. The slope of the absorption edge measures the degree of order, which in turn depends on the Ni concentration in the films.

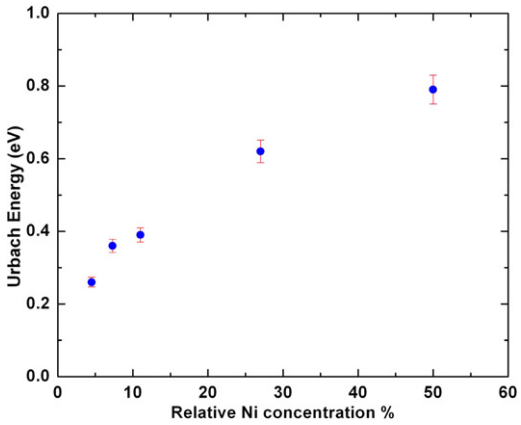

Figure 5. Urbach slope as a function of Ni concentration.

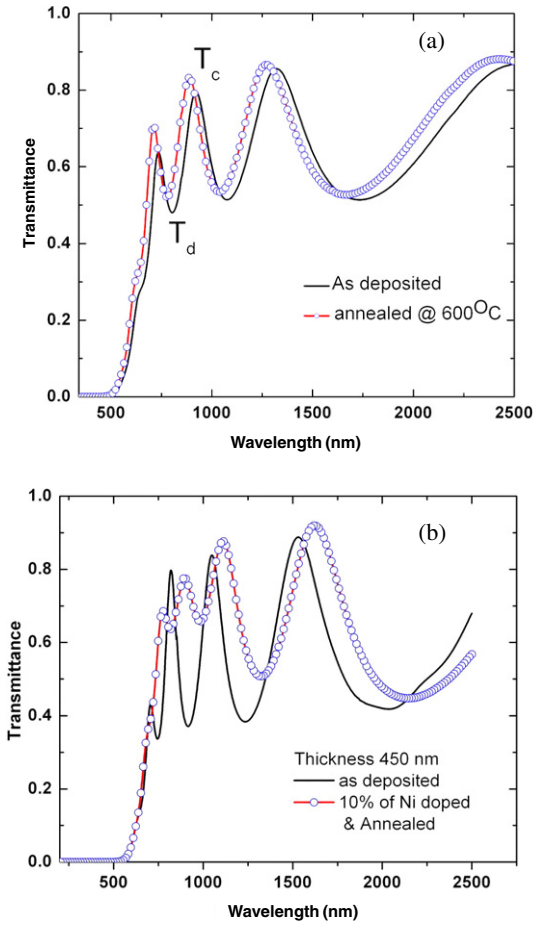

Figure 6. Spectral transmission curves of (a) as-deposited films and (b) the films after Ni doping and annealing to a temperature of 600 °C.

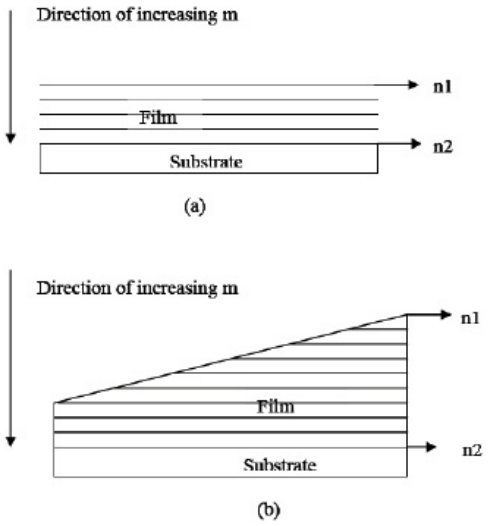

Figure 7. (a) Schematic of an optically homogeneous thin film showing the increasing order of interference, m, and refractive indices $n1$ and $n2$ at the film–air and film–substrate interfaces, respectively. Here $n1 = n2$. (b) Schematic of an optically inhomogeneous thin film showing the increasing order of interference, m, and refractive indices $n1$ and $n2$ at the film–air and film–substrate interfaces respectively. Here $n1 \neq n2$.

The films showed a variation in the band gap from 1.6 to 1.89 eV, clearly indicating confinement effects due to the nanocrystallinity. These values demonstrate the possibility of tailoring the band gap of MIC silicon over a wide range of values. Another interesting feature is that the band gap of the annealed undoped and doped Si films displays very little variation in their values in spite of the annealing process. The implication of this in the context of the local electronic structure in the presence of Ni will be discussed using the refractive index data to be presented later.

The effect of Ni doping on the system has also been studied using the spectral transmission curves as shown in figure 6. The spectral transmittance of the pure a-Si films as-deposited and those annealed at 600 °C are shown in figure 6(a). The spectral transmittance for the films doped with a Ni concentration of 11% and annealed is shown in figure 6(b). It is evident from the figures that while the positions and the absolute values of transmittance at points of constructive and destructive interference (indicated by T_c and T_d, respectively, in figure 6(a)) do not vary significantly as a result of annealing in the undoped Si films, for the Ni doped films there is a significant change in the features of the transmittance spectra. The first significant deviation in behavior is that the T_d values in the case of the doped films are wavelength dependent. For a completely optically homogeneous film, the T_d and T_c values remain constant in the dispersion-free region of refractive index, as observed in figure 6(a). However, for optically inhomogeneous films, both the values and the wavelengths at which T_c and T_d occur will differ from that of the corresponding homogeneous film. Optically homogeneous films are those that possess thickness and wavelength independent refractive indices in the dispersion-free region of the spectrum. The origin of inhomogeneity can be traced to the structural, microstructural and chemical inhomogeneities along the thickness (i.e. the cross-section) of the film. Such a film is modeled as having a wedge shape rather than the flat parallel faces as is assumed for homogeneous films. A schematic of this is shown in figure 7.

The inhomogeneous film can then be further modeled as a multilayered structure consisting of several interfaces each of which has a different refractive index at a given wavelength. This

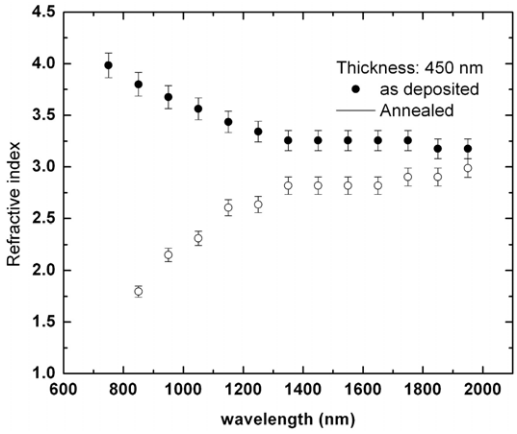

Figure 8. Variation in the refractive index due to Ni content and annealing as a function of wavelength λ.

leads to a film with a gradient in refractive index across its cross-section of thickness rather than a single refractive index for the entire cross-section at a given wavelength, as is the case for homogeneous films. The calculated dispersion in refractive index '*n*' for the a-Si films with and without Ni is shown in figure 8. The dispersion for the annealed undoped Si film shows the idealized behavior with increase in refractive index in the region of the band gap and constant value in the dispersion-free region between 1200 and 2500 nm. The nickel doped film, on the other hand, shows anomalous behavior in the dispersion of refractive index. It exhibits a decreasing refractive index in the region of the band gap while remaining constant in the dispersion-free region. The decrease in refractive index is accompanied by an increase in absorption coefficient, which indicates that the contribution to the refractive index in this region is from the other component of the films such as metal or metal silicides.

Since, in the dispersion-free region, the refractive indices of the undoped and doped films are 3.4 and 3.2, respectively, these values originate from the unreacted Si components of the film. The value compares favorably with that of crystalline Si films and can therefore be attributed to the unreacted nanocrystalline Si component of the film. The contribution of the metal silicide clearly affects the region of the band gap and therefore the band structure. That this is a consequence of the diffusion process can also be inferred from the condition for constructive interference

$$2nd = m\lambda \tag{3}$$

where n is the refractive index of film of thickness d at a wavelength λ and m is the order of interference. The left-hand side of equation (3) is also known as the optical thickness. The order of interference, m, increases with decrease in wavelength and, more importantly, the interference at higher values of m originates closer to the substrate–film interface than the film–air interface. Based on this argument, from the spectral transmission curves in figure 6 and the dispersion curve in figure 8 it is clear that Ni diffusion occurs from the surface in to the bulk of the film. During the process of diffusion, the Ni catalyzes the crystallization process as Si atoms migrate to the surface. As a consequence, there is optical inhomogeneity in the film characterized by anomalous dispersion in the refractive index. It would thus appear that most of the crystalline Si is on the surface of the film and that the majority of the Ni diffuses into the bulk. This would also explain the lack of crystallinity in films doped with relatively larger concentrations of Ni (>5%). Secondly, it would appear that in the case of the

evaporated films the crystallization is driven by the rate of reaction at the interface rather than the diffusion process, and hence the crystallization occurs within the first 15–20 min of the annealing process. The diffusion process dominates thereafter, since further annealing does not improve the crystallinity in the current case.

4. Conclusions

The process of Ni metal induced crystallization of amorphous silicon thin films is followed using Raman scattering and UV–vis–NIR spectrophotometry. A detailed study of the transmittance, reflectance and optical absorption spectra reveals the presence of signatures of crystallization in them, previously unreported for MIC-Si. Crystallization causes inhomogeneity in spectral transmission behavior leading to optical inhomogeneity that can be traced to structural and compositional variations along the thickness of the films. This is also manifested in the anomalous dispersion in refractive index. In specular reflectance the appearance of peaks at 3.3 and 4.4 eV shows that crystallization has occurred, and these can be compared with Raman spectra that are used traditionally for establishing crystallization. A detailed analysis of the absorption spectra reveals variations in Urbach edges that can be correlated with the crystallization process. The crystallization temperature is of the order of 600 °C for 4.5% relative concentration of Ni. It is thus demonstrated that an optical study of MIC can reveal many details and provide insights into the process that is often not possible with other probes in a non-destructive fashion.

Acknowledgments

The authors acknowledge the financial support from the Department of Science and Technology India–Trento Program for Advanced Research (DST-ITPAR) program. One of the authors (KUMK) would like to thank the DST-ITPAR for providing a Bose-Romagnosi fellowship to do this work. Facilities provided by the University Grants Commission under UPE and SAP programs are gratefully acknowledged. We wish to thank Dr P S R Prasad, National Geophysical Research Institute, Hyderabad for invaluable help in Raman spectroscopy measurements.

References

[1] Ayers J R, Botherton S D and Young N D 1991 *Solid State Electron.* **34** 671
[2] Mayer J W, Eriksson L, Picraux S T and Davies J A 1968 *Can. J. Phys.* **46** 663
[3] Choi J H, Kim D Y, Kim S S, Park S J and Jang J 2003 *Thin Solid Films* **440** 1
[4] Giust G K, Sigmon T W, Boyce J B and Ho J 1999 *IEEE Electron Device Lett.* **20** 77
[5] Liu G and Fonash S J 1993 *Appl. Phys. Lett.* **62** 254
[6] Pereira L, Aguas H, Martins R M S, Vilarinho P, Fortunato E and Martins R 2004 *Thin Solid Films* **451** 334
[7] Dimova-Malinovska D 2005 *J. Optoelectron. Adv. Mater.* **7** 99
[8] Jin Z, Bhat G A, Yeung M, Kwok H S and Wong M 1998 *J. Appl. Phys.* **84** 194
[9] Swanepoel R 1983 *J. Phys. E: Sci. Instrum.* **16** 1214
[10] Ghanashyam Krishna M and Bhattacharya A K 1997 *Mater. Sci. Eng.* B **49** 166
[11] Brodsky M H, Cardona M and Cuomo J J 1977 *Phys. Rev.* B **16** 3556
[12] Iqbal Z and Veprec S 1982 *J. Phys. C: Solid State Phys.* **15** 377
[13] Mishra P and Jain K P 2001 *Phys. Rev.* B **64** 073304
[14] Richter H and Ley L 1981 *J. Appl. Phys.* **52** 7281
[15] Campbell I H and Fauchet P M 1986 *Solid State Commun.* **58** 739
[16] Pisanec S, Contoro M, Ferrari A C, Zapien J A, Lifshitz Y, Lee S T, Hofmann S and Robertson J 2003 *Phys. Rev.* B **68** 241312(R)

[17] Schubert E, Fahlteich J, Rauschenbach B, Schubert M, Lorenz M, Grudmann M and Wagner G 2006 *J. Appl. Phys.* **100** 016107
[18] Peter Y Yu and Cardona M 2004 *Fundamentals of Semiconductors: Physics and Materials Properties* 3rd edn (Berlin: Springer) pp 243–4
[19] Phillip R H and Ehrenreich H 1963 *Phys. Rev.* **129** 1550
[20] Kane O E 1966 *Phys. Rev.* **146** 558
[21] Zanattam A R, Mulato M and Chambouleyron I 1998 *J. Appl. Phys.* **84** 5184
[22] Zanatta A R and Chambouleyron I 1996 *Phys. Rev.* B **53** 3833
[23] Cody G D 2005 *Mater. Res. Soc. Symp. Proc.* **862** A1.3.1
[24] Urbach F 1953 *Phys. Rev.* **92** 1324